

# Recent evolution of an ice-cored moraine at the Gentianes Pass, Valais Alps, Switzerland

Ludovic Ravanel<sup>1,2</sup> | Pierre-Allain Duvillard<sup>2,3</sup>  | Michel Jaboyedoff<sup>4</sup> | Christophe Lambiel<sup>1</sup>

<sup>1</sup>IDYST, University of Lausanne, Lausanne, Switzerland

<sup>2</sup>Université Grenoble Alpes, USMB, CNRS, EDYTEM, Chambéry, France

<sup>3</sup>IMSRN, Montbonnot, France

<sup>4</sup>ISTE, University of Lausanne, Lausanne, Switzerland

## Correspondence

L. Ravanel, Université Grenoble Alpes, USMB, CNRS, EDYTEM, F-73376 Le Bourget du Lac, France.

Email: ludovic.ravanel@univ-smb.fr

## Abstract

Lateral moraines located in permafrost environments often preserve large amounts of both glacier and periglacial ice. To understand how ice-cored moraines located in high alpine environments evolve in a context of both glacier retreat and permafrost degradation, we performed 11 terrestrial laser-scanning measurement campaigns between 2007 and 2014 on a highly anthropogenic overprinted moraine prone to instability. Resulting comparison of the subsequent 3D models allowed to qualitatively and quantitatively analyze the morphological evolution of the moraine. The comparisons indicate a very high geomorphic activity of the moraine including large areas affected by downslope movements of blocks and 10 landslides with a volume between  $24 \pm 1$  and  $1,138 \pm 47 \text{ m}^3$ . Data also indicated a very strong ice melt with a loss of ice thickness locally reaching 17.7 m at the foot of the moraine. These results, compared with resistivity and thermal measurements of the ground, suggest the combined role of ice loss at the foot of the moraine and the permafrost activity/warming in triggering these processes.

## KEYWORDS

anthropogenic overprinting, ice-cored moraine, paraglacial, permafrost warming, Valais Alps

## 1 | INTRODUCTION

With the current disturbance of geosystems due to temperature increase over the last decades, changes in high mountain environments have become reliable indicators of climate change, and in particular the phenomena of glacier retreat (Oerlemans, 2005; Zemp et al., 2015) and permafrost warming (Harris et al., 2009; PERMOS, 2016). The latter, which has been studied more recently (Haeberli et al., 2010), refers to the warming of any ground types that remain at or below 0°C for at least two consecutive years. Both processes, and a combination of the two, are often used to explain the current increase in gravity-related events (rockfalls and landslides) in high mountains (Ravanel & Deline, 2011; Ravanel, Magnin, & Deline, 2017). On high-altitude rockwalls typical of areas around alpine glaciers, permafrost warming—which greatly reduces the shear strength of discontinuities when ground temperatures approach 0°C—is one of the main triggering factors for rockfalls (Draebing, Krautblatter, & Dikau, 2014; Fischer, Purves, Huggel, Noetzli, & Haeberli, 2012;

Gruber & Haeberli, 2007). The combination of this degradation and glacial retreat—which reduces buttressing, that is, support of slopes—can also cause instabilities whose magnitude can vary greatly depending on geological and cryospheric parameters (McColl & Davies, 2013; Ravanel, Allignol, Deline, Gruber, & Ravello, 2010; Sailer et al., 2012). This combination can then affect the stability of moraines in the periglacial belt (Lukas, Nicholson, Ross, & Humlum, 2005; Mortara & Chiarle, 2005; Tonkin, Midgley, Cook, & Graham, 2016).

Such instabilities and the related land degradation increase as the climate warms (Haeberli, 1992; Kääb, Reynolds, & Haeberli, 2005). This is of special concern for high alpine mountains with significant infrastructure (mountain huts, railways, cable cars, and associated buildings; Duvillard, Ravanel, & Deline, 2015) that are experiencing an increase in the numbers of visitors (tourists). In recent years, an increasing amount of damages has occurred on existing structures, both on bedrock (Ravanel, Deline, Lambiel, & Vincent, 2012) and loose sediments (Phillips et al., 2007; Springman & Arenson, 2008), and in particular on glacial landforms and sediments.

To assess how alpine ice-cored moraines currently evolve, we carried out investigations on a moraine whose relevance is increased because of the presence of ski infrastructure on it. Ice-cored moraines, as transitional landforms, are altered while de-icing (Lukas, 2011; Lukas et al., 2005; Østrem, 1959), underlining the geomorphic sensitivity of high-altitude environments to climate change (see Harrison, 2009; Knight & Harrison, 2012). Two types of melting have been described for ice-cored moraines: downwasting and backwasting (Kjær & Krüger, 2001). The latter is the dominant process in high-Arctic areas and corresponds to the melting of free ice-cliffs and debris-covered slopes. It is generally accompanied by debris flows, gravity sorting, and melt pond formation (Lukas, 2011; Lukas et al., 2005; Schomacker & Kjær, 2008). Unlike in high-Arctic areas, where most of the studies were made, little attention has been paid to alpine lateral ice-cored moraines. In alpine context, studies focussed on the interactions between glaciers and permafrost (e.g., Bosson & Lambiel, 2016; Kneisel, 2003; Reynard et al., 2003; Ribolini et al., 2010); on ice-free moraines (Mortara & Chiarle, 2005); or on ice-cored moraines out of permafrost area (Ackert, 1984; Brook & Paine, 2012), whereas some authors have associated ice-cored moraines with rock glaciers (Barsch, 1971). It is therefore necessary to identify processes at work during a de-icing period as today.

The study site is a highly anthropogenic overprinted ice-cored moraine located at the Gentianes Pass (2,894 m asl) in the Swiss Alps (Valais), on which two cable car stations and a restaurant have been built. The moraine has been extensively excavated during various phases of construction work and is now affected by a very high activity on its inner flank. The latter was monitored using high spatial and temporal resolution terrestrial laser scanning (TLS) between 2007

and 2014. Eleven measurement campaigns were carried out and complete kinematic data obtained by differential Global Navigation Satellite System (dGNSS) survey between 2004 and 2009. The TLS method is currently standard but still not much used in high alpine environments (Arenson, Kääb, & O'Sullivan, 2016; Ravanel, Deline, & Jalliet, 2011), even for the monitoring of sedimentary formations (Avian, Kellerer-Pirkbauer, & Bauer, 2009; Bodin, Schoeneich, & Jalliet, 2008; Ravanel, Bodin, & Deline, 2014).

This study aims to determine in detail the magnitude of the type of mass movements that affect the moraine and to analyse these movements in terms of ground ice/glacier ice characteristics and distribution as well as retreat of the adjacent glacier.

## 2 | STUDY SITE

The study area (Figure 1) is located on the left bank of the Rhone Valley (Valais Alps, Switzerland), at the limit between the Bagnes and the Nendaz valleys. Geologically, the area belongs to the Mont Fort nappe (Escher, 1988; Schaer, 1960), one of the main units of the Pennine Alps. This base layer is generally composed of gneiss from a marked Paleozoic metamorphism (Gouffon & Burri, 1997). Because of their location, the Valais Alps are under the influence of an intra-alpine continental climate, due to air masses drying as they pass over the alpine foothills to the west (most low-pressure areas come from the west), meaning that annual precipitation is relatively low (Currie, Sands, & Porter, 2009). This is reflected at high altitude by the limited presence of glaciers and, as a consequence, by the development of large periglacial landforms (rock glaciers and talus slopes). The current mean

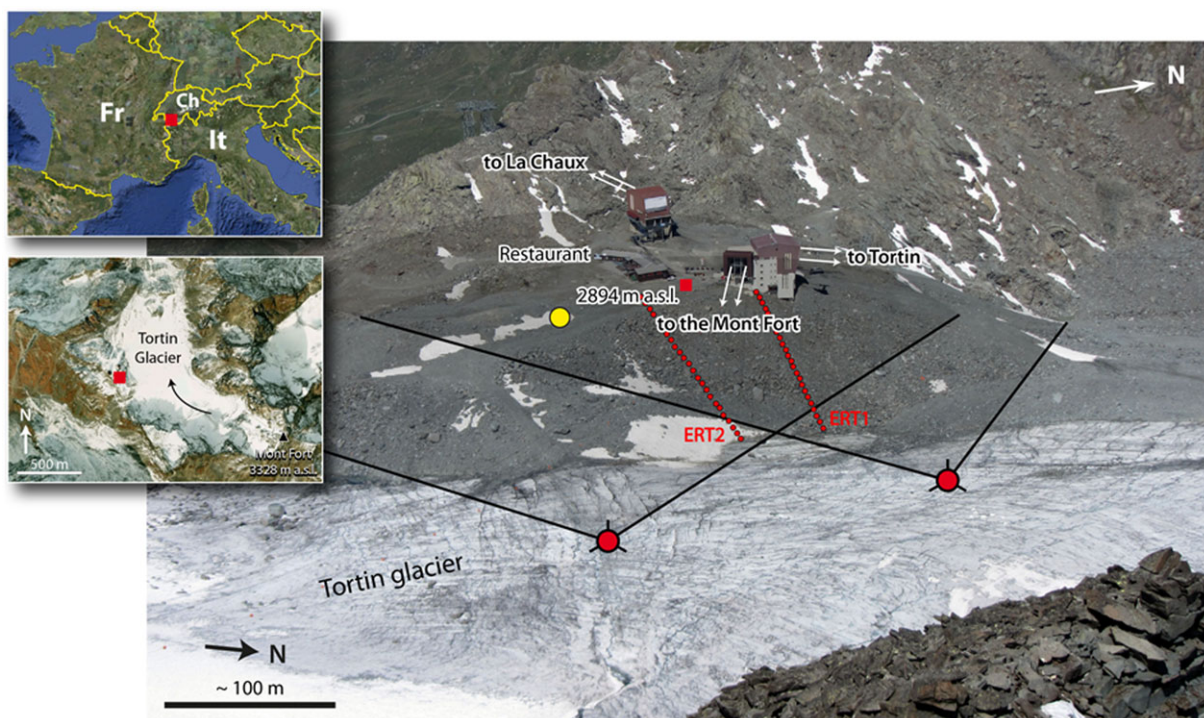


**FIGURE 1** The Gentianes moraine (Valais Alps, Switzerland) and its infrastructure. The inner flank (east flank) is scanned from two main locations, approximately positioned here. The yellow dot indicates instrumented borehole and measurement of the air temperature. The aligned red dots indicate electrical resistivity tomography profiles [Colour figure can be viewed at [wileyonlinelibrary.com](http://wileyonlinelibrary.com)]

annual air temperature at the Gentianes pass is around  $-1^{\circ}\text{C}$  (mean 2007–2017).

The Gentianes Pass (2,880 m asl) is dominated by Mont Fort (3,328 m asl), whose NW face shades the upper part of the small Tortin glacier ( $\sim 0.8 \text{ km}^2$ ), which retreated on around 1,000 m since the end of the nineteenth century (Glaciological Reports, 1881). The Gentianes moraine, orientated south–north, corresponds to the left lateral moraine of this glacier and marks its Little Ice Age (LIA) position (Lambiel & Schuetz, 2008). The glacier is currently still in contact with the moraine. In the study area, its inner flank (east flank) reaches a height of about 50 m, with a mean slope of around  $35^{\circ}$ .

The site has been used for skiing since the late 1970s. The bottom station of the Mont Fort cable car was built on the moraine between 1977 and 1979. Difficulties with the construction were encountered due to the presence of massive ground ice (Lambiel, 2006). To prevent movement of the building, six 2.5-m-wide concrete pillars were buried in the frozen ground to an average depth of 15 m. Additional excavation works carried out in October 2006 on the path leading from the buildings to the glacier revealed the presence of massive ground ice at several places at depth varying from 0.5 to 2 m (Lambiel & Schuetz, 2008). Observations and analyses of ice samples showed the coexistence of both sedimentary and congelation ice, the former indicating that glacier ice was incorporated in the moraine.

These successive levelling works greatly modified the initial shape of the moraine. Previously, its southern part was a large, rounded, and elongated hillock, suggesting that it had formed by the deformation of frozen sediments due to the advancing Tortin glacier during the LIA.

### 3 | METHODS

TLS is the main method used in this study. This technology is used in several ways in geomorphology, that is, mapping, geometry, and monitoring (Abellán, Derron, & Jabyedoff, 2016; Jabyedoff et al., 2012). Regarding the latter, relatively few studies have been conducted in high mountain environments (Bhardwaj, Sam, Bhardwaj, & Martín-Torres, 2016; Bodin et al., 2008; Oppikofer, Jabyedoff, Blikra, Derron, & Metzger, 2009; Oppikofer, Jabyedoff, & Keusen, 2008; Rabatel,

Deline, Jallet, & Ravanel, 2008; Ravanel et al., 2011, 2014). With this study, TLS is used for the first time to monitor an ice-cored moraine for a long period.

To discuss the results obtained by TLS with regard to the evolution of the site, several complementary methods were implemented: air temperature measurement, depth of the active layer measurement (top layer that thaws every year), and imaging subsurface structures of the moraine by electrical resistivity tomography (ERT).

#### 3.1 | Terrestrial laser scanning

Changes in the moraine surface were first studied seasonally with dGPS (GNSS) between 2004 and 2009, before the survey with TLS only. The first TLS measurements at the Gentianes Pass were carried out in July 2007. Since then, the moraine has been scanned once (2009, 2012, 2013, and 2014); twice (2007 and 2008); or three-times (2011) a year (with a break in 2010; Table 1), from two or three locations.

We used an Optech ILRIS 3D (wavelength: 1,500 nm). The scanning distance was  $\sim 270$  m, which is within the device range of 500 to 600 m. According to the manufacturer, the precision of the obtained model is 7 mm for the distance and 8 mm for the position at 100 m. There is a lack of critical review of the ILRIS 3D characteristics, but this precision remains consistent with different tests done with other scanners Leica, Mensi, Riegl, Faro, or Z+F (Boehler, Bordas Vicent, & Marbs, 2003; Gordon, Lichti, Stewart, & Tsakiri, 2000; Gumus & Erkaya, 2011).

Five to 10 scenes (depending on the scan position and overlapping performed by the operator) are acquired from two or three points of view (Figure 1) to cover the slope, with considerable overlap between them ( $\sim 30\%$ ) to enable the coregistration of the 3D models.

We obtained 3D models from point clouds using InnovMetric PolyWorks software. To create a 3D model, two scenes—consisting of one or more 3D images—are first assembled from the recognition of 'n pairs of corresponding points' (at least 3) identified in the two scenes. These points are matched, allowing an initial coregistration, then improved using the 'best fit' tool with an iterative algorithm (Eggert, Fitzgibbon, & Fisher, 1998) based on the Iterative Closest Point method (Besl & McKay, 1992). This method minimizes the

**TABLE 1** 3D model characteristics

3D model	Date of acquisition (MM-DD-YYYY)	Number of point clouds	Number of points	Mean point spacing (mm)
July 2007	7-19-2007	8	12,589,596	47.2
October 2007	10-16-2007	9	9,518,515	54.2
July 2008	7-30-2008	8	52,889,147	23.0
October 2008	10-1-2008	6	23,697,114	34.4
September 2009	9-18-2009	10	15,692,020	42.2
July 2011	7-3-2011	6	15,055,263	43.1
August 2011	8-30-2011	7	21,194,600	36.3
October 2011	10-17-2011	9	7,906,099	59.5
October 2012	10-5-2012	5	16,253,548	41.9
October 2013	10-3-2013	7	19,587,235	38.7
October 2014	10-20-2014	9	24,598,348	33.8
Total		84	218,981,485	
Mean		7.5	19,907,408	41.3

distance between two-point clouds that overlap (Oppikofer et al., 2009; Rabatel et al., 2008). The average point spacing (Table 1) was between 23.0 and 59.5 mm. Except when snow was particularly prevalent (in October 2007 and 2011, for example), these variations did not affect the quality of the 3D models. When the coregistration is complete, all the point clouds are in the (local) coordinate system of the first imported scene. Georeferencing was carried out for the last model (2014) using points acquired with a GNSS Trimble GEO7X in September 2015. As the whole moraine is rapidly changing, only the 5 points acquired on the cable car station—which is stable as indicated by the topographic surveys ordered by the operator—were kept. This georeferencing only allowed measurement of the overall slope angle and altitudes. However, as this georeferencing was not performed directly during every LiDAR acquisition, it could not be used to properly align the different models during the comparison stage.

We also used PolyWorks to obtain the comparison map of high resolution 3D models (Adams & Chandler, 2002; Ravanel et al., 2010; Young & Ashford, 2006), the analysis of which provides the opportunity to identify areas of instability (Abellan et al., 2014). Once a morphological change has been identified, it can be measured kinetically (block moved and manually tracked) or volumetrically (landslide; for the method, see Ravanel et al., 2010). The most minor changes are considered similar to a lack of change (same color, i.e., grey) by the use of a buffer thickness of 20 cm (up to  $\pm 10$  cm); no smaller scale movement detection is needed, contrary to other studies (e.g., Kromer et al., 2015). This buffer also helps to overcome the instrumental, environmental, and coregistration errors.

The issue of uncertainties has been taken into account in fluvial geomorphology (Lane, Chandler, & Richards, 1994; Lane, Westaway, & Hicks, 2003; Wheaton, Brasington, Darby, & Sear, 2010), but relatively less elsewhere (Lichti, Gordon, & Tipdecho, 2005; Oppikofer et al., 2009). It is nevertheless essential to avoid erroneous calculations and interpretations.

A total uncertainty can be estimated by the quadratic sum of the different independent stochastic errors throughout acquisition and data processing (Baltsavias, 1999; Milan, Heritage, & Hetherington, 2007; Rabatel et al., 2008). The total uncertainty is mainly due to errors related to the scanner itself ( $\sigma_1$ ), scanned objects ( $\sigma_2$ ), environment ( $\sigma_3$ ), and methods ( $\sigma_4$ ; Reshetuk, 2006), and corresponds to

$$\sigma_{\text{tot}} = \sqrt{\sigma_1^2 + \sigma_2^2 + \sigma_3^2 + \sigma_4^2}.$$

For instrument errors ( $\sigma_1$ ; see Boehler et al., 2003; Schulz & Ingensand, 2004; Lichti & Licht, 2006), we used those provided by the manufacturer (7 mm at 100 m). The reflectivity of the gneiss being generally high (Zhao, Yan, Zhao, Lv, & Wu, 2007), errors associated with scanned objects ( $\sigma_2$ ) may be neglected. As with any optical measurement of distance, changes in light propagation speed due to changes in temperature and pressure can affect results. Similarly, noise may result from beam scattering due to wind and humidity. Surveys at high altitude, however, provide reasonably good conditions of acquisition (dry and stable weather, no dust). Errors associated with the environment ( $\sigma_3$ ) may also be neglected, especially as the roughness of the slope on a large scale optimizes the angle of incidence of the laser beams (Lichti & Harvey, 2002). Errors related to the methods ( $\sigma_4$ ) used should

therefore be the most significant, although those due to model georeferencing have been eliminated. The main errors thus come from coregistration when the 3D models are created and when they are aligned. However, the various adjustments have greatly minimized this (Hodgetts, 2009): The alignment obtained is in the order of 10 mm. Another quality check of the 3D image/model alignment is done by comparing the 3D models themselves. In the case of important coregistration errors, the comparison over time of these models would reveal significant morphological changes. But these changes are no longer detectable with the use of the  $\pm 10$ -cm-thick buffer—in which any instrumental and environmental errors are also included. The maximum total uncertainty would finally be  $\sim 23$  mm and would affect almost exclusively the axis perpendicular to the surface. Because they involve variations on this axis, volume calculations must take into account this uncertainty: The maximum uncertainty for a detached volume is the value of the product of the uncertainty for both models ( $\sim 46$  mm after averaging the point error) and the surface affected by the detachment.

Uncertainty was additionally quantified using straight and stable east wall of the cable car station, which is normal to the scanning direction. A plane was fitted to the points on the wall, and uncertainty was calculated as a derivation of points from the plane. For a given model, a plane can already be used to quantify the instrumental errors by studying the point-to-plane distances. The average standard deviation obtained was 18 mm, and 98% of the points were located within twice this standard deviation: The maximum error is thus 36 mm. But this value does not only reflect instrumental errors: It also includes errors due to the type of surface being scanned, the environmental errors, and the 3D image alignment errors. For the first type of error, it was assumed that the errors identified on concrete are identical to those on gneiss. The second was difficult to quantify independently. The last was considered negligible with regard to the alignment reports. For each comparison, the planes were then exported to calculate the root-mean-square errors; the average root-mean-square error was 11 mm. We thus obtained a total uncertainty of 47 mm with the “immobile plane” method, which was consistent with the method by the quadratic sum of individual errors. This also suggested that we do not need to take into consideration environmental errors and those related to the type of scanned surface.

### 3.2 | Ground and air temperature measurement

A 21-m-deep borehole was drilled in 2002 around 120 m south of the main cable car station (Lambiel, 2006). Below 1.5 m of unfrozen sediment, a 1.5-m-thick layer of massive ice was found, below which 15-m frozen debris (mixture of ice, gravels and pebbles) were present. The bedrock was not reached. The borehole was then equipped with a plastic tube, in which ground temperatures are recorded each 2 hr since the drilling with a Multi Datalogger (MADD Technologies; accuracy:  $\pm 0.1^\circ\text{C}$ , resolution:  $0.01^\circ\text{C}$ ) and 11 sensors located at increasing downhole depth interval: -0.5, -1.0, -1.5, -2.3, -3.6, -5.09, -7.08, -9.57, -12.56, and -20.04 m. The data are included in the Swiss Permafrost Monitoring Network PERMOS (PERMOS, 2016).

Air temperature is recorded hourly at the Gentianes pass since October 2007 by a miniature temperature logger UTL-1 (accuracy:  $\pm 0.1^\circ\text{C}$ ; resolution:  $0.22^\circ\text{C}$ ) in the shadow of the cable car station.

### 3.3 | Electrical resistivity tomography

ERT is a method commonly used to detect and map permafrost and ground ice, because the ground resistivity increases with ice content and with decreasing temperatures below 0°C (Emmert & Kneisel, 2017; Hauck, Vonder Mühl, & Maurer, 2003; Hilbich, Marescot, Hauck, Loke, & Mäusbacher, 2009). Resistivity ranges from few kΩm for frozen sediments to more than 1 MΩm for sedimentary ice. Ice content and origin can thus be assessed according to the measured values. The resistivity is obtained by injecting electric current into the ground and by measuring its intensity and the resulting potential difference. The apparent resistivity must then be inverted to get the specific resistivity of each layer.

Several ERT profiles have been carried out since 2007 in the study area in order to characterize the internal structure of the moraine and to map the extent of ground ice (Lambiel & Baron, 2008; Lambiel & Schuetz, 2008). We used for this study two 92-m-long ERT profiles (depth penetration up to ~15 m) carried out in August 2009 in the inner flank of the moraine. A Wenner-Schlumberger configuration was chosen, and for each profile, 24 electrodes with 4-m intervals were disposed, which gives a profile length of 92 m. The survey was carried out with a Syscal Pro Switch system (*Iris Instruments*). The raw data were processed with the software Prosys and were finally inverted with the software RES2DINV (Loke & Barker, 1996).

## 4 | RESULTS

### 4.1 | Morphological evolution of the moraine between 2007 and 2014

TLS data acquired between 2007 and 2014 have allowed 10 3D model comparisons over time to be carried out (Figures 2.1 and 2.2; Table 2). The wavelength used is not appropriate for ice detection, but at the foot of the moraine, the ice is partly covered by debris, which allowed an indirect detection.

The first comparison (July–October 2007; Figure 2.1a) reveals that the ice at the foot of the moraine had been affected by a thickness loss of 2.10 m on its south side, because the microtopography is essentially the same on the two models (very little reorganization). On the left half of the image, the apparent loss of thickness is due to the melting of late-lying snow patches. On the moraine itself, several changes are noteworthy. The most directly visible one is a landslide of  $198 \pm 6 \text{ m}^3$  for which the detachment, transit, and deposition zones are clearly identifiable. In the detachment zone, the coarse material exported downhill was replaced on the surface by a much finer grained material. The debris layer that has been removed reached a depth locally of 1.85 m. Positive volume changes (sediment accumulation) appear on both sides of this landslide. The volume of the southern one is  $705 \pm 65 \text{ m}^3$ . Finally, about 20 m downstream from the cable car station, a 40-m-wide and 15-m-high area is characterized by downslope movements of blocks [0.95 (1.75) m] (notation [X (Y)]: X is an average value, and Y is a maximum value).

Between October 2007 and July 2008, morphodynamics decreased in intensity (Figure 2.1b), although in the northern part of

the comparison, the average loss in ice thickness at the foot of the moraine was still significant (~1.65 m). The only significant change in the moraine is visible at the north of the building and corresponds to the reworking of previously deposited materials.

The third comparison (Figure 2.1c) shows changes that occurred during summer 2008 (July–October). The image evidences a further significant loss of ice thickness (~1.35 m). Meanwhile, a new landslide occurred just south of the summer 2007 one. Identified through the triptych scar, transit, and deposit zones, it mobilized  $111 \pm 6 \text{ m}^3$  of material to a maximum depth of 1.35 m. Two other areas were affected by movements of blocks: in the area already affected in 2007 [1.45 (2.35) m] and further to the north [1.20 (1.35) m], in a smaller area.

The following comparison (Figure 2.1d) probably shows changes, which occurred during summer 2009 as it compares the 3D model of October 2008 with that of September 2009. During this period, the loss of ice thickness generally continued (~1.75 m). On the northern part of the study area, new deposits occurred. Three areas were affected by movements of blocks: The common one, located to the south, is the largest [0.4 (0.8) m]; to the north, the area, which had been affected during the previous period, was reorganized again [1.15 (1.80) m]; between these two, a sector was also—to a lesser extent—affected by movements [0.25 (0.45) m]. Downhill from the latter, two juxtaposed landslides occurred with a total volume of  $1,138 \pm 47 \text{ m}^3$ , revealing massive ice (Figure 3a). The maximum depth of detachment was observed in the ‘north’ slide (1.45 m).

Although no measurements were carried out in 2010, the following comparison (September 2009 to July 2011; Figure 2.1e) likely indicates the morphogenic activity during summer 2010. Further loss of ice thickness at the foot of the moraine is recorded (~0.85 m). The two main areas of individual block movements continued to evolve ([1.05 (1.15) m] for the northern area and [1.15 (1.50) m] for the southern), with a substantial expansion on the south. Between these two sectors, a significant loss of volume was recorded ( $874 \pm 61 \text{ m}^3$ ). Thickness loss locally was up to 1.50 m.

Summer 2011’s activity (early July–late August; Figure 2.2f) was significant. As well as the loss of ice thickness (~0.50 m), there was a deposit made close to the cable car station, and the continuation of the movement of blocks in the areas outlined above, with three landslides occurring on the moraine. From south to north, the first one ( $270 \pm 12 \text{ m}^3$ ) occurred within the main sector of unstable blocks (Figure 3b). The maximum depth of detachment was 1.95 m. The second volume of material ( $217 \pm 14 \text{ m}^3$ ) was destabilized only a few meters below the infrastructure to a maximum depth of 1.6 m. Further north, the third landslide mobilized  $546 \pm 20 \text{ m}^3$  of material to a maximum depth of 2.45 m in a small area. The last two landslides also revealed large areas of massive ice (Figure 3b).

The following comparison (Figure 2.2g) illustrates the evolution of the study area during late summer 2011 (August–October). Due to snowfall, which preceded data acquisition, evolution of ice at the foot of the moraine was not quantifiable. On the moraine, three areas continued to be affected by block movements ([0.90 (1.05) m], [0.60 (1.35) m] and [0.55 (0.95) m] from south to north), particularly in the area affected by the landslides during summer 2011. Small readjustments (falling blocks) affected the head of the starting zone

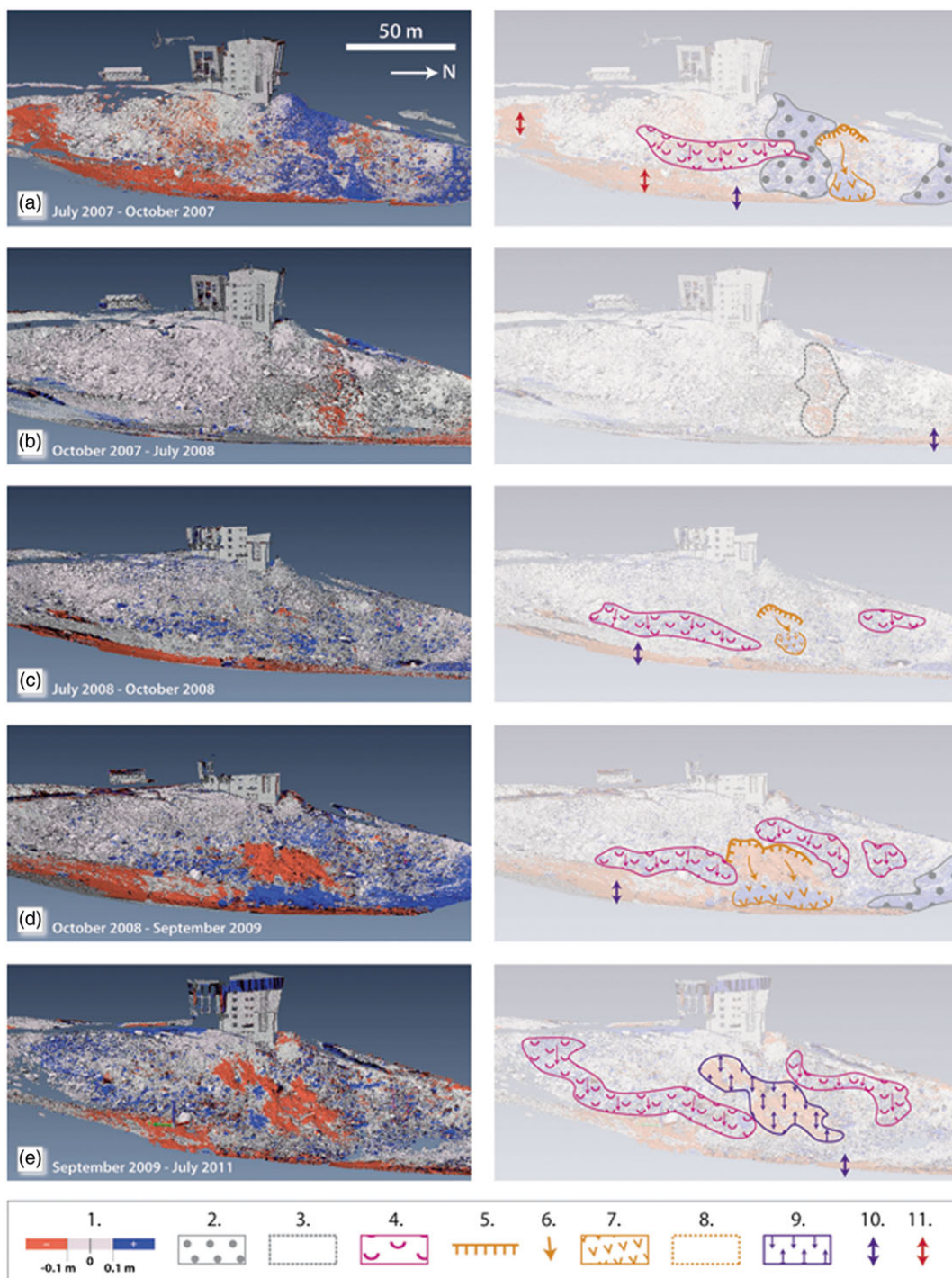


**FIGURE 2.1** The first five comparisons over time of 3D models acquired between 2007 and 2011 in the Gentianes area (left) and their geomorphological significance (right). North is on the right. 1: The moraine is affected by positive or negative volume changes. A  $\pm 10\text{-cm-thick}$  buffer left in grey corresponding to a lack of change is applied (see text). 2: Deposits of anthropogenic origin; 3: compaction of anthropogenic deposits; 4: downslope movements of blocks; 5: scars; 6: landslide transit zone; 7: landslide deposit zone; 8: readjustments (block falls); 9: loss of volume by ice melt. 10: loss of glacier thickness; 11: loss of thickness due to snowmelt [Colour figure can be viewed at [wileyonlinelibrary.com](http://wileyonlinelibrary.com)]

at the same time. A later landslide, whose volume is estimated to be around  $115\text{ m}^3$  (no precise volume could be measured due to the presence of snow), also affected this area, which had already seen a lot of activity over the summer with a landslide of  $270\text{ m}^3$ .

Between October 2011 and October 2012 (Figure 2.2h), while block movements continued in the northern and southern areas ( $[0.6$  ( $1.2\text{ m}$ ) and  $[0.7$  ( $1.0\text{ m}$ ), respectively], the situation became dynamic

beneath the cable car station where two small slides ( $24 \pm 1$  and  $70 \pm 4\text{ m}^3$ ) occurred, a large block moved  $2.2\text{ m}$  and a volume of  $914 \pm 41\text{ m}^3$  went 'missing.'

The penultimate comparison illustrates the evolution of the moraine between October 2012 and October 2013 (Figure 2.2i). This period was marked by low-intensity movements, although the ice in this area still lost between  $-0.75$  and  $-1.8\text{ m}$  in thickness. However,

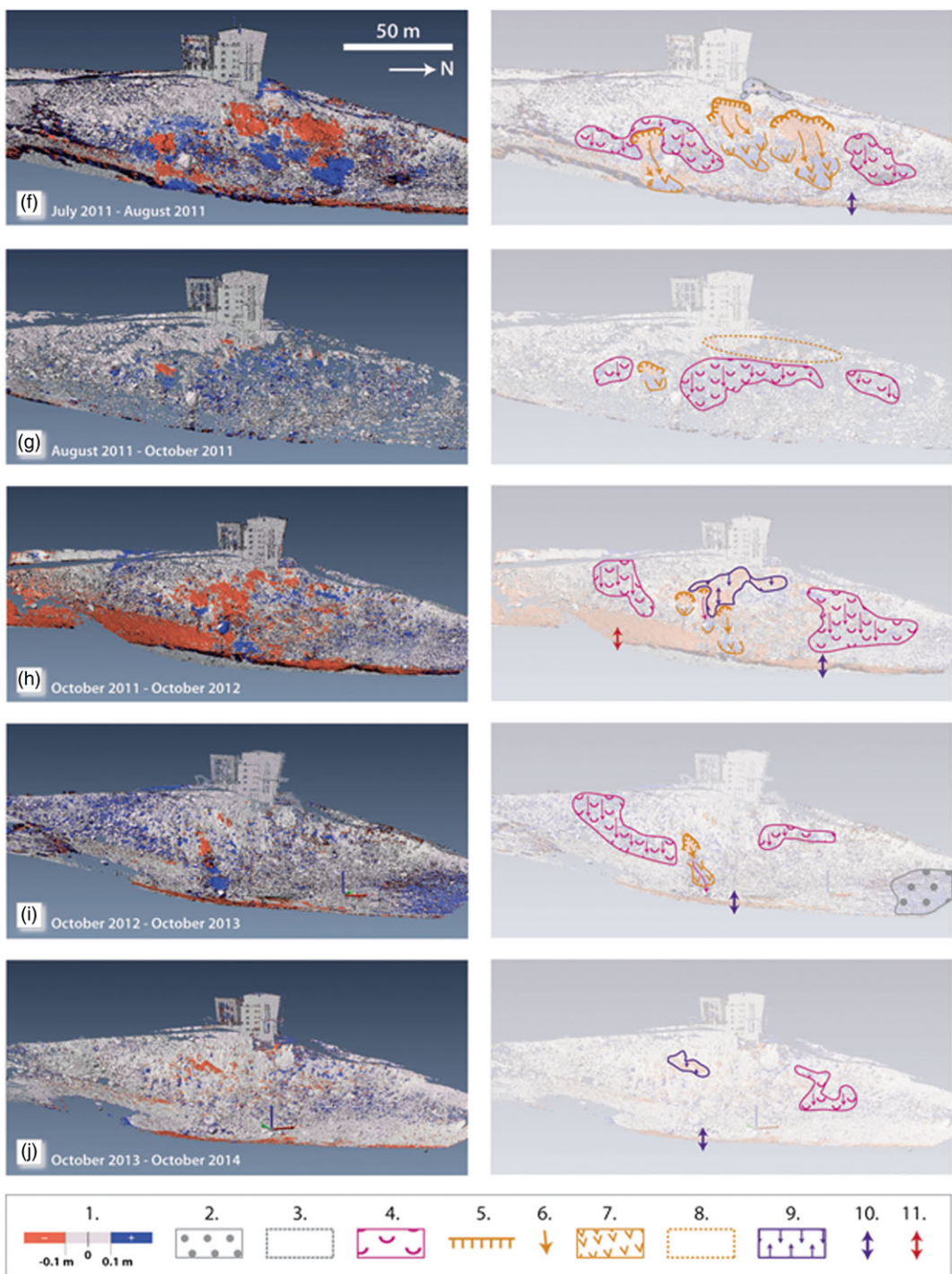


**FIGURE 2.2** The last five comparisons over time of 3D models acquired between 2011 and 2014 in the Gentianes area (left) and their geomorphological significance (right). See Figure 2.1 for caption [Colour figure can be viewed at [wileyonlinelibrary.com](http://wileyonlinelibrary.com)]

to the south, a broad sector continued to be affected by block movements [0.55 (1.3) m]. The big block that had moved more than 2 m in the previous period moved even more with a displacement of 22.5 m. It was accompanied by a small slide of  $84 \pm 4 \text{ m}^3$ . New deposits were also made in the far north of the study area.

The last comparison reflects the activity of summer 2014 (October 2013 to October 2014; Figure 2.2j). This remained particularly low, the ice level decreasing by only 0.80 m. Block movements [1.0 (3.3) m] were relatively rare and mainly occurred in the northern part. A small area experienced a loss of volume of  $54 \pm 3 \text{ m}^3$ , due to ice melting.

## 4.2 | Internal structure of the moraine

The main process, which has occurred on the moraine flank, is the sliding of unconsolidated debris. Field observations show that the slides occurred systematically at the surface of an ice layer (Figure 3), which is characterized by a high content of air bubbles. This indicates that it is sedimentary ice (see Haeberli & Vonder Mühl, 1996; Shumskii, 1964), that is, glacier ice still present within the moraine.

ERT1, carried out below the cable car station, shows resistivity values higher than 1,000 kΩm at the base of the moraine (Figure 4),

**TABLE 2** Main instabilities identified on the inner flank of the Gentianes moraine between 2007 and 2014

3D model comparison	Corresp. summer	Volume change (m <sup>3</sup> )	Affected area (m <sup>2</sup> )	Max. thickness ( $\pm 0.05$ m)	Mean thickness (m)	Depth of the permafrost active layer (m)
July–October 2007	2007	198 $\pm$ 6	135	1.85	1.40	1.5
July–October 2008	2008	111 $\pm$ 6	125	1.35	0.90	No data
October 2008 to September 2009	2009	1,138 $\pm$ 47	1,000	1.45	1.20	2.1
September 2009 to July 2011	2010	874 $\pm$ 61 <sup>a</sup>	1,300	1.50	0.70	2
July–October 2011	2011	270 $\pm$ 12 217 $\pm$ 14 546 $\pm$ 20 ~115 <sup>b</sup>	1,033 $\pm$ 46 250 300 425 140	1.95 1.60 2.45 1.15	1.10 0.75 1.30 0.80	3.1
October 2011 to October 2012	2012	24 $\pm$ 1 70 $\pm$ 4	94 $\pm$ 5 35 85	1.30 1.80	0.75 0.85	3
October 2012 to October 2013	2013	84 $\pm$ 4	100	1.65	0.90	4
October 2013 to October 2014	2014	Ø				4.4

<sup>a</sup>Negative change in volume without establishment of a deposit (ice melt).

<sup>b</sup>Indirect quantification due to the presence of snow.



**FIGURE 3** Massive ice with the presence of air bubbles (lower half on ph. (a) and bottom left on ph. (b)) revealed in landslide starting zones. (a) Starting zone of the two juxtaposed landslides of 1,138  $\pm$  47 m<sup>3</sup> (see Figure 2.1d; photo: 5 October 2009); (b) northern margin of the starting zone of the 270  $\pm$  12 m<sup>3</sup> landslide (see Figure 2.2f; photo: 30 August 2011) [Colour figure can be viewed at [wileyonlinelibrary.com](http://wileyonlinelibrary.com)]

indicating the presence of glacier ice (e.g., Kulessa, 2007). The values decrease toward the top of the moraine but remain higher than 100 k $\Omega$ m under a 2-m-thick debris cover on a large part of the profile. This supports the observations that massive ice is present in most of the landslide detachment zones. A significant decrease in resistivity (less than 4 k $\Omega$ m) was observed at the base of the cable car station, which probably corresponds to ice-free sediments (e.g., Thompson, Kulessa, & Luckmann, 2012).

ERT2 (Figure 4) reveals also the presence of debris-covered glacier ice at the base of the moraine, but the values measured higher in the slope remain largely lower than on ERT1. They are indeed comprised between 8 and 15 k $\Omega$ m below a 3- to 5-m-thick unfrozen surface layer. Such values are interpreted as frozen sediments, without massive ice layers (Emmert & Kneisel, 2017; Lambiel & Schuetz, 2008).

#### 4.3 | Temperature variations over time

In the Gentianes area, apart for 2007 for which no temperature data are available, the hottest year was 2011 ( $-0.3^{\circ}\text{C}$ ; Figure 5). Summers 2009 and 2012 were the warmest of the study period (mean

temperature of the 90 consecutive warmest days:  $6.7$  and  $7.0^{\circ}\text{C}$ , respectively) and summer 2014 was the coldest ( $4.9^{\circ}\text{C}$ ). If we look at the hottest period (10-day period) of each year, mean temperatures were between  $7.9^{\circ}\text{C}$  (2014) and more than  $11^{\circ}\text{C}$  (2010, 2011, and 2012). The hottest day occurred in 2012 with a temperature of  $14.4^{\circ}\text{C}$ . Years 2009, 2011, and 2012 would thus appear to be the most prone years for geomorphic activity related to high temperatures. There is a lot of variation in the dates when these high summer temperatures occurred early June in 2014; end of June in 2008; early July in 2010; mid-July in 2010; end of July/beginning of August in 2013; and end of August in 2009, 2011, and 2012. The potential for destabilization corresponding to those periods of high temperatures is not comparable from one year to another, depending on whether they occurred during snowmelt or at times when the moraine had been completely snow-free for several weeks.

Temperatures measured in the borehole indicate the presence of permafrost conditions in the moraine (Lambiel, 2006; PERMOS, 2016). In 2007, the temperatures at 20-m depth were at  $-0.5^{\circ}\text{C}$  and experienced then a continuous warming to reach  $-0.27^{\circ}\text{C}$  in October 2014 (Figure 6). The temperatures were more stable during the 5 years

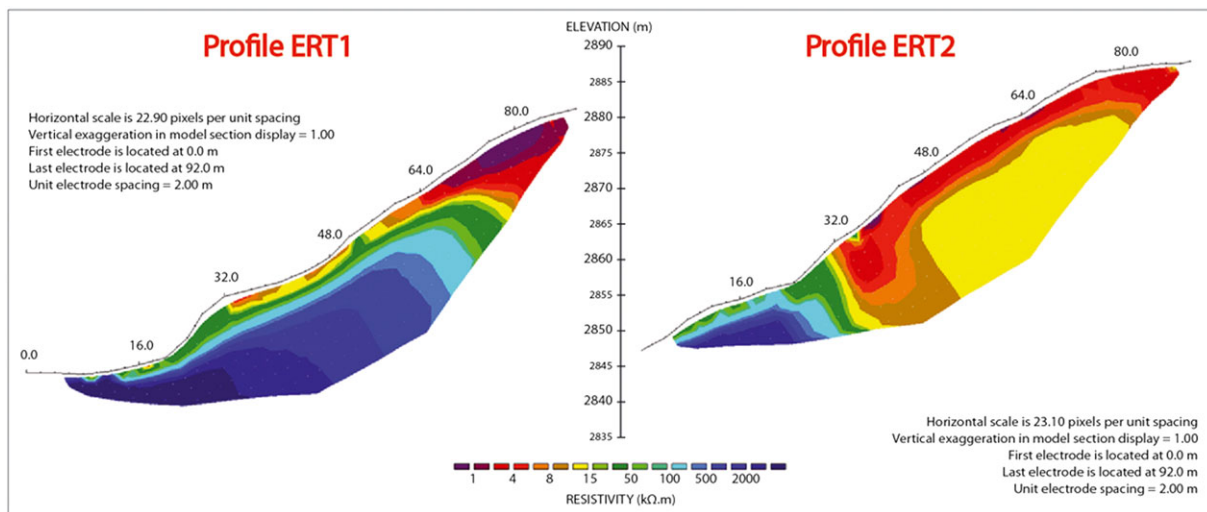


**FIGURE 4** Two electrical resistivity profiles measured in August and October 2009, respectively, in the inner flank of the Gentianes moraine. For location, see Figure 1 [Colour figure can be viewed at [wileyonlinelibrary.com](http://wileyonlinelibrary.com)]

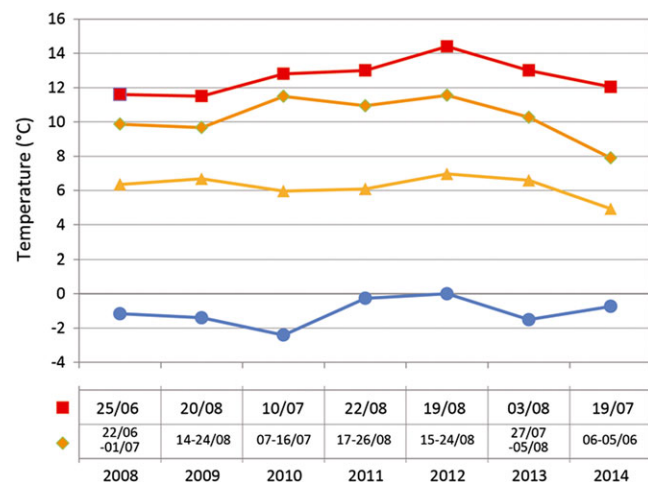


**FIGURE 5** Variation in air temperature at the Gentianes pass. The blue dots represent mean annual air temperature; the triangles represent mean air temperature of the 90 consecutive warmest days of the year; the rhombus represents mean temperature of the 10 consecutive hottest days of the year; the squares represent mean temperature of the warmest day of the year. Dates (DD/MM) in the lower part of the document correspond to the dates of the hottest days and of the 10 consecutive hottest days of each year [Colour figure can be viewed at [wileyonlinelibrary.com](http://wileyonlinelibrary.com)]

before the study period, varying between  $-0.54^{\circ}\text{C}$  (2002) and  $-0.4^{\circ}\text{C}$  (2006). The active layer remained stable at a thickness of 1.5 m up to 2007 before the initiation of a major and rapid deepening. In fall 2014, its thickness was indeed 4.4 m.

## 5 | DISCUSSION

Comparison of the 3D models revealed that the inner flank of the Gentianes moraine is affected by a high level of geomorphic activity, as it is sometimes the case in high-Arctic (Ewertowski & Tomczyk, 2015). Negative volume changes (excluding loss of glacier ice) reached almost  $5,500 \text{ m}^3$ . In this section we aim to discuss their origin.

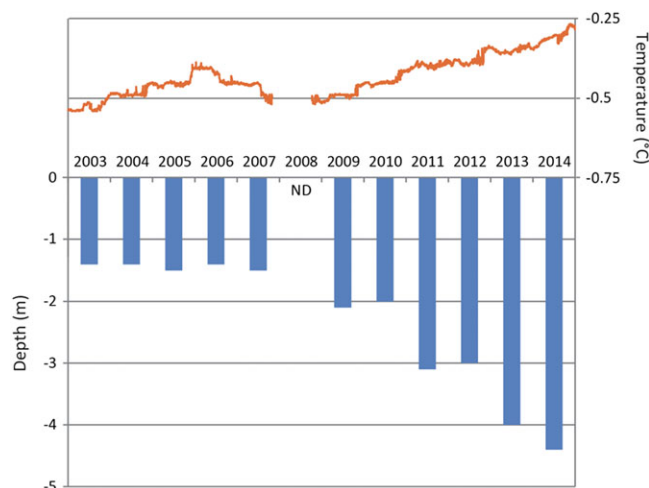


**FIGURE 6** Evolution of the active layer thickness of the permafrost measured in the borehole (histogram) of the Gentianes moraine (2,880 m asl), compared to ground surface temperature (line) [Colour figure can be viewed at [wileyonlinelibrary.com](http://wileyonlinelibrary.com)]

### 5.1 | Evolution directly imposed by anthropogenic action

Direct observations or works reported by site managers indicate that few measured changes are of human origin. These are mainly deposits of materials related to maintenance work on the glacier access path. Both the positive volume changes of the summer 2007 are related to deposits of anthropogenic origin resulting from important excavations on the path at the end of the summer. Between October 2007 and July 2008, negative changes on the later deposits correspond to their compaction/reorganization. During summer 2009 and 2011 and between October 2012 and October 2013, other deposits of anthropogenic origin occurred. They are all related to new phases of excavation of the path. The material is generally evacuated in the northern part of the slope, often from a platform located in the immediate vicinity of the station. The blocks roll and slide on the slope, often up to its foot. In both cases, one thus obtains overaccumulation of materials,

which can produce a landslide at the time of their deposit or later. The deposits of summer 2007 (see Section 4), which are by far the largest ( $>700 \text{ m}^3$ ), were potentially able to trigger—or to participate in triggering—the 198-m<sup>3</sup> landslide of the summer 2007. In the case of landslide prior to deposition, this landslide would have been obliterated. In addition, the materials remaining in the slope could be mobilized during the following years. Overload of the upper parts of the slope can indeed change slope instability and trigger a landslide: Dynamic effects reduce the shear strength of the debris layer and generate additional stress decreasing the slope stability (Van Den Eeckhaut, Poesen, & Hervás, 2013).

## 5.2 | A paraglacial evolution

The Tortin Glacier has been retreating continuously since the end of the LIA. It has lost more than 1 km in length and 2.6 km<sup>2</sup> in surface since 1878. Today, its length is only ~1.3 km, and its surface is ~0.70 km<sup>2</sup>. In 2014, the maximum thickness measured with ground-penetrating radar (Nobes, 2011) was 42 m (GEOSAT SA, unpublished

data). Except for years 2013 and 2014, no snow was still present at the surface of the glacier, indicating that the glacier has had no accumulation zone in recent years. The small size of this glacier makes it thus extremely sensitive to current warming.

The Gentianes moraine is prone to instability in this context of glacial retreat. The very significant reduction in ice thickness measured by TLS (up to -2.10 m between July and October 2007 and up to 17.7 m in total between 2007 and 2014; Figure 7) could explain—at least partly—the recent geomorphic activity of the moraine: Landslides and downslope movements of blocks could be partly attributed to a loss of buttress (Geertsema & Chiarle, 2013). This activity could be described as ‘paraglacial’ in the sense of Church and Ryder (1972) that is, unstable conditions caused by a significant relaxation time in processes and geomorphic patterns following glacial climates. When the glacier loses thickness, the base level of the ice surface is lowered, and lateral sedimentary formations can be destabilized (Ballantyne, 2002a, 2002b; McColl, 2012). This phenomenon is possibly even more apparent when the slope angle increases (Claessens, Temme, & Schoorl, 2013; Ewertowski & Tomczyk, 2015), as it is the case for

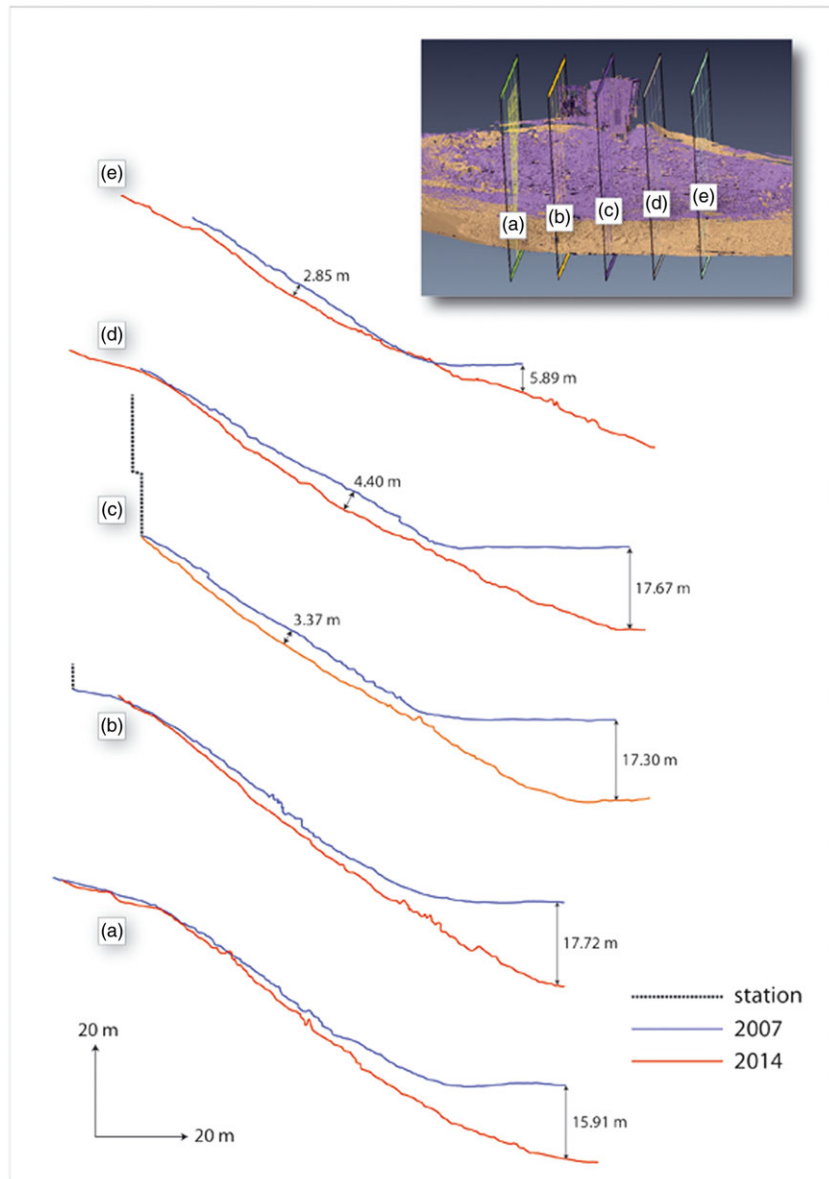


**FIGURE 7** Comparison 2007–2014 of five cross sections extracted from the TLS models of the Gentianes moraine. In 7 years, the slope has locally lost up to 4.4 m thick. Thickness loss of the glacier locally reaches 17.7 m in the same period [Colour figure can be viewed at [wileyonlinelibrary.com](http://wileyonlinelibrary.com)]

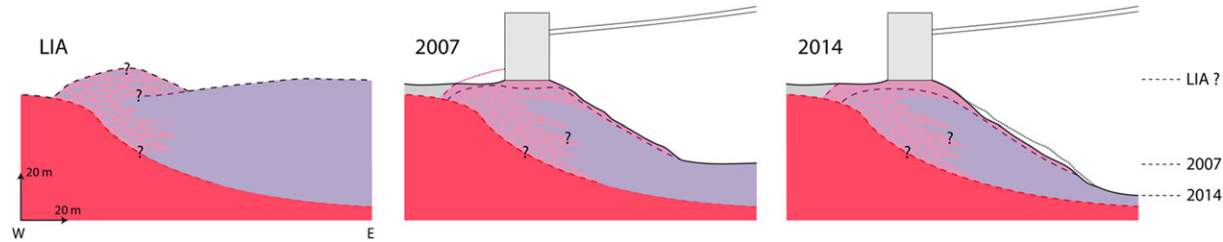


**FIGURE 8** Model of evolution of the Gentianes moraine since the Little Ice Age. The push moraine (in mauve), whose implementation was completed during the LIA, still covers a part of the Tortin Glacier (in purple), thus locally limiting the ice melt. The building and the embankment appear in grey. Close to the surface, mauve without purple ellipses corresponds to the active layer [Colour figure can be viewed at [wileyonlinelibrary.com](http://wileyonlinelibrary.com)]

the Gentianes moraine, where the mean slope increased from  $31.6^\circ$  to  $35.7^\circ$  between 2007 and 2014 (Figure 7).

Below the cable car station, where the landslides occurred, ERT1 profile showed the presence of glacier ice (presence of air bubbles). Ice was also generally visible in the scars of the landslides (bare-ice conditions; Figure 3). So directly exposed at the surface, ice can melt (dead-ice melting; Schomacker, 2008) and explain rapid loss of thickness, as the loss of volume of  $874 \text{ m}^3$  during summer 2010. The absence of deposits at the foot of the moraine suggests that this is not due to another landslide but to the melting of the ice uncovered by the landslide of the previous period, with a reorganization of the rock material still present on the ice (microtopography not preserved). It was also the case with the 'missing' volume of  $914 \text{ m}^3$  between October 2011 and October 2012. According to the geoelectrical data, this ice layer has a consistent thickness. In this sector (Figure 8), glacier ice is indeed still present as the Tortin glacier has experienced less intense melting in recent years than the rest of the glacier (Brook & Paine, 2012; Deline, 2005). Dead ice of glacial origin embedded within the moraine is thus an element of the paraglacial adjustment, in the sense of Ballantyne (2002a) or Jäger and Winkler (2012). The presence of ice-free sediments recognized through ERT1 at the base of the cable car station can be explained either by local warming due to heat exchange between the building and the ground—the cable car station is not equipped with any system which may limit this phenomenon—or/and by the fact that excavation work required for anchoring the building to the moraine has resulted in an accelerated melting of the frozen material. The existence of the building has an influence on ground ice, whereas the subsidence of the moraine had already been observed during the digging of the foundations. Anyhow, the retreat of the glacier and the presence of glacier ice under a relatively thin superficial debris layer, acting as sliding plane, appears to be one of the main factor at the origin of the landslides. However, it cannot be the sole explanation, even less so with regard to the movements of blocks in the absence of the creep/thawing of the superficial layer of the moraine.

### 5.3 | A periglacial evolution

The combination of the high altitude of the moraine and the fact that geomorphic activity is greater in summer tends to support the role of thawing in triggering the activity documented in this paper. Over 7 years, summers appear to be the main periods of activity (landslides

and block movements), although some of the comparisons include changes, which may have occurred in winter (October 2008 to September 2009 for example). This high level of summer activity has also been observed (a) with previous kinematic measurements carried out by dGPS (Lambiel & Schuetz, 2008); (b) through field observations; (c) by managers of the ski area, sensitized to our study; and (d) a survey of the moraine with an automatic camera since summer 2012. Moreover results from the only "winter" comparison (October 2007 to July 2008) indicate that the moraine underwent no changes other than a reorganization of the deposits accumulated over the previous period. This seasonality corresponds to what is usually observed on rock glaciers (e.g., Buchli, Merz, Zhou, Kinzelbach, & Springman, 2013) and high-Artic ice-cored moraines (Ewertowski & Tomczyk, 2015): Movements are higher in summer, correlated with an increase in ground temperatures (Delaloye, Lambiel, & Gärtnert-Roer, 2010) that increase permafrost creep (Haeberli et al., 2006). On the moraine, the creep is illustrated by the downslope movements of blocks, very effective in the southern and northern parts, that is, on both sides of the central sector, which is mainly affected by landslides. In these two sectors apart from each other, the presence of permafrost conditions was confirmed by borehole temperatures and various observations of ground ice during excavation works. In the southern area affected by the movements of blocks, the ERT2 profile suggests the absence of glacier ice. In this case, we are probably in the presence of ice-supersaturated materials, similar to rock glaciers, and block movements can be fairly explained by the likely creep of supersaturated frozen moraine.

Relaying during the summers with this probable creep, the annual thawing of the surface layer and the interannual evolution of the permafrost active layer is in position of reinforcing the dynamics of the previously creep-affected areas. Indeed, the temperature measurements in the borehole indicate a very rapid deepening of the active layer between 2007 and 2014:  $+2.9 \text{ m}$  in 7 years, that is, an increase in thickness of the seasonally thawing ground by 300% even if we must remain circumspect because of possible sources of errors (accuracy and arrangement of sensors, ground subsidence, and excavation nearby; see Luethi & Phillips, 2016). This rapid warming is corroborated by temperature measurements at 20 m in depth, where the thermal signal is nevertheless much lower ( $+0.23^\circ\text{C}$  over the study period). We are thus in presence of very sensitive permafrost (Magnin et al., 2015). This general warming illustrated by a deeper active layer suggests that a part of the downslope movements affecting the moraine

could be attributed to the solifluction in the sense of a plug-like flow originating from annual freeze-thaw action (Matsuoka, 2001), possibly reinforced by water from precipitation. Magnitude of the movements measured (often  $>1 \text{ m.yr}^{-1}$ ) tends to reinforce the hypothesis of a coupling of the two processes, but solifluction and permafrost creep are probably independent (Gorbunov & Seversky, 1999) in time (early summer as opposed to late summer) and mechanics (flow of saturated sediments as opposed to the flow of ice-rich sediments). In high-Arctic, Bennett and French (1991) have shown that the coupling of the two processes can lead to sliding.

The landslides that we measured in the central part of the study area could thus constitute the ultimate phase of development of the downslope movements of blocks. This development is here allowed by the presence of glacier ice at shallow depth, acting as sliding plane. To trigger the slide, it is necessary for the layer of sediment covering the ice to thaw. During the study period, although it should be emphasized that the borehole is not located in the area where the main geomorphic activity occurs, it is noteworthy that the mean depth of detachment of the landslides is generally much shallower than the active layer depth. Summer thawing of the entire sediment layer up to the glacier ice is another condition for its detachment and the development of a landslide.

A last important parameter explaining the landslides very probably intervene: the liquid water content. Landslides usually occur during the warmest periods of the summer, which induce a deepening of the active layer and the melting of the glacier ice at the base of the debris. The consequential lubrication of the surface of the impermeable ice then acts as a triggering factor for the landslides. A second favorable context is summer storms, which greatly increase the water content in the debris over a short time all the way to the level of the ice. Likely elevated pore-water pressures at the base of the layer of debris probably lead to its destabilization. Although the frequency of TLS acquisitions does not allow to definitively validate this hypothesis, many elements support it. The presence of a high water content in the sliding mass is, for example, suggested by the shape of the deposit of the 198-m<sup>3</sup> landslide of the summer 2007, with a very marked and lobed front. Heavy rains can act on the moraine slope through two physical mechanisms. The first is simply the weight of the extra water (overload), which tends to push sediments downhill; the second is more important: The extra water raises the water pressure inside the pores of the landslide mass (Dikau, 2013). However, contrary to what is regularly observed in high-Arctic regarding the evolution of ice-cored moraines, we did not observe the development of sediment-flow fans (Bennett, Huddart, Glasser, & Hambrey, 2000; Ewertowski & Tomczyk, 2015; Lukas et al., 2005), probably due to the reduced amounts of sediments available at the Gentianes moraine and the reduced dimensions of the slope. On the other hand, the rates of erosions can be comparable: dead-ice melting and mass wasting processes can reach more than 1.8 m.yr<sup>-1</sup> in Svalbard (Ewertowski & Tomczyk, 2015), whereas the measured maximum thickness of the Gentianes landslides can be up to 1.80, one time up to 2.45 m. As in high Arctic (Bennett et al., 2000; Ewertowski & Tomczyk, 2015; Kjær & Krüger, 2001; Lukas et al., 2005), the most important process, which led to the transformation of the Gentianes ice-cored moraines, is gravitational mass movement.

## 6 | CONCLUSIONS

The 10 comparisons over time of 3D models acquired by TLS between 2007 and 2014 at the Gentianes moraine showed a general trend towards instability and land degradation in the area, especially between 2007 and 2012, with a very high activity between 2009 and 2011.

In particular, the following are observed:

- The moraine experiences significant geomorphic activity: in addition to the anthropogenic deposition of material, the moraine is affected by significant downslope movements of blocks as well as landslides. A further loss of volume results from melting ice.
- About  $3,650 \pm 175 \text{ m}^3$  of material have been destabilized during this period.
- The 3D model comparisons also showed a high degree of glacier melting throughout the study period. Locally, this reached a depth of close to 18 m, which corresponds to a local ablation of around 2.50 m.yr<sup>-1</sup>.

As well as the changes due to the construction and operation of the tourist infrastructure (mainly overaccumulation of materials), this high geomorphic activity can mainly be explained by the combination of the following:

- A paraglacial context corresponding to the loss of buttress related to the loss of glacier ice thickness (up to 17.7 m) together with an increase of the slope angle (from 31.6° to 35.7° in 7 years); the presence of glacier ice under the debris layer is otherwise acting as sliding plane for landslides.
- A periglacial dynamic allowing the likely creep of the frozen moraine while the annual thawing of the active layer and its inter-annual evolution (deepening) might generate plug-like flow.

Landsliding, a process already recognized as very important in the degradation of high-Arctic ice-cored moraines facing global warming, correspond to the last phase of development of the instability of the moraine, probably favoured by the thaw/lubrication of the surface of the impermeable underlying permafrost table. Multiple processes are acting together, delaying surface stabilisation.

The plurality of methods developed at the Gentianes moraine offers a unique insight in the ice-cored moraine degradation and associated processes. It also demonstrates its suitability for studies of alpine permafrost and illustrates the scale of the risk to a major tourist area of the Valais Alps. This study gives credit to Bommer, Phillips, Keusen, and Teyssiere (2010), who concluded that if a building situated on ice-rich permafrost is to remain structurally viable, looking for another construction site should be considered as an option.

## ACKNOWLEDGMENTS

The authors would like to thank the Téléverbier and Télénendaz companies for allowing access and facilitating this work, as well as François-Joseph Baillifard, Benoît Mazotti, François Riff, Stefan Utz, and Charles Grange for their help on the field. They would also like

to thank Neil Brodie for improving the English. This paper is part of the ongoing EU-POIA *PermaRisk* project.

## ORCID

Pierre-Allain Duvillard  <http://orcid.org/0000-0001-7698-2985>

## REFERENCES

- Abellan, A., Derron, M. H., & Jaboyedoff, M. (2016). Use of 3D point clouds in geohazards: Current challenges and future trends. *Remote Sensing*, 8, 130. <https://doi.org/10.3390/rs8020130>
- Abellan, A., Oppikofer, T., Jaboyedoff, M., Rosser, N. J., Lim, M., & Lato, M. J. (2014). Terrestrial laser scanning of rock slope instabilities. *Earth Surface Processes and Landforms*, 39, 80–97. <https://doi.org/10.1002/esp.3493>
- Ackert, R. P. (1984). Ice-cored lateral moraines in Tarfala Valley, Swedish Lapland. *Geografiska Annaler A*, 66, 79–88. <https://doi.org/10.2307/520940>
- Adams, J. C., & Chandler, J. H. (2002). Evaluation of LiDAR and medium scale photogrammetry for detecting soft cliff coastal change. *The Photogrammetric Record*, 17, 405–418. <https://doi.org/10.1111/0031-868X.00195>
- Arenson, L. U., Kääb, A., & O'Sullivan, A. (2016). Detection and analysis of ground deformation in permafrost environments. *Permafrost and Periglacial Processes*, 27, 339–351. <https://doi.org/10.1002/ppp.1932>
- Avian, M., Kellerer-Pirkbauer, A., & Bauer, A. (2009). LiDAR for monitoring mass movements in permafrost environments at the cirque Hinteres Langtal, Austria, between 2000 and 2008. *Natural Hazards and Earth System Sciences*, 9, 1087–1094. <https://doi.org/10.5194/nhess-9-1087-2009>
- Ballantyne, C. K. (2002a). A general model of paraglacial landscape response. *The Holocene*, 12, 371–376. <https://doi.org/10.1191/0959683602hl553fa>
- Ballantyne, C. K. (2002b). Paraglacial geomorphology. *Quaternary Science Reviews*, 21, 1935–2017. [https://doi.org/10.1016/S0277-3791\(02\)00005-7](https://doi.org/10.1016/S0277-3791(02)00005-7)
- Baltsavias, E. P. (1999). Airborne laser scanning: Basic relations and formulas. *ISPRS Journal of Photogrammetry and Remote Sensing*, 54, 199–214. [https://doi.org/10.1016/S0924-2716\(99\)00015-5](https://doi.org/10.1016/S0924-2716(99)00015-5)
- Barsch, D. (1971). Rock glaciers and ice-cored moraines. *Geografiska Annaler A*, 53, 203–206. <https://doi.org/10.1080/04353676.1971.11879846>
- Bennett, L. P., & French, H. M. (1991). Solifluction and the role of permafrost creep, Eastern Melville Island, N.W.T., Canada. *Permafrost and Periglacial Processes*, 2, 95–102. <https://doi.org/10.1002/ppp.3430020204>
- Bennett, M. R., Huddart, D., Glasser, N. F., & Hambrey, M. J. (2000). Resedimentation of debris on an ice-cored lateral moraine in the high-Arctic (Kongsvegen, Svalbard). *Geomorphology*, 35, 21–40. [https://doi.org/10.1016/S0169-555X\(00\)00017-9](https://doi.org/10.1016/S0169-555X(00)00017-9)
- Besl, P. J., & McKay, N. D. (1992). A method for registration of 3-D shapes. *IEEE Transactions on Pattern Analysis and Machine Intelligence*, 14, 239–256. <http://www.cs.virginia.edu/~mjh7v/bib/Besl92.pdf>
- Bhardwaj, A., Sam, L., Bhardwaj, A., & Martin-Torres, F. J. (2016). LiDAR remote sensing of the cryosphere: Present applications and future prospects. *Remote Sensing of Environment*, 177, 125–143. <https://doi.org/10.1016/j.rse.2016.02.031,2016>
- Bodin X, Schoeneich P., & Jalliet S. (2008). High-resolution DEM extraction from terrestrial LiDAR topometry and surface kinematics of the creeping alpine permafrost: the Laurichard rock glacier case study (southern French Alps). Proceedings of the 9<sup>th</sup> International Conference on Permafrost, Fairbanks, Alaska 1: 137–142. <http://research.iarc.uaf.edu/NICOP/DVD/1st%20to%209th%20Conference%20PDF%20files/09th%20International%20Conference%20on%20Permafrost%20Extended%20Abstracts.pdf>
- Boehler, W., Bordas Vicent, M., & Marbs, A. (2003). Investigating laser scanner accuracy. *The International Archives of the Photogrammetry, Remote Sensing and Spatial Information Sciences*, 34, 696–701.
- Bommer, C., Phillips, M., Keusen, H. R., & Teysseire, P. (2010). *Bauen im permafrost*. (p. 126). Switzerland: WSL, Birmensdorf. <http://www.slf.ch/dienstleistungen/buecher/9819.pdf>
- Bosson, J. B., & Lambiel, C. (2016). Internal structure and current evolution of very small debris-covered glacier systems located in alpine permafrost environments. *Frontiers in Earth Science*, 4, 39. <https://doi.org/10.3389/feart.2016.00039>
- Brook, M. S., & Paine, S. (2012). Ablation of ice-cored moraine in a humid, maritime climate: Fox Glacier, New Zealand. *Geografiska Annaler A*, 94, 339–349. <https://doi.org/10.1111/j.1468-0459.2011.00442.x>
- Buchli, T., Merz, K., Zhou, X., Kinzelbach, W., & Springman, S. (2013). Characterization and monitoring of the Furggwanghorn rock glacier, Turtmann valley, Switzerland: results from 2010 to 2012. *Vadose Zone Journal*, 12, 1–15. <https://doi.org/10.2136/vzj2012.0067>
- Church, M., & Ryder, J. M. (1972). Paraglacial sedimentation: A consideration of fluvial processes conditioned by glaciation. *GSA Bulletin*, 83, 3059–3072. [https://doi.org/10.1130/0016-7606\(1972\)83\[3059:PSACOF\]2.0.CO;2](https://doi.org/10.1130/0016-7606(1972)83[3059:PSACOF]2.0.CO;2)
- Claessens, L., Temme, A. J. A. M., & Schoorl, J. M. (2013). Mass-movement causes: Changes in slope angle. Mass-movement causes: Overloading. In: Stoffel M, Marston RA. (dir.). In *Treatise on Geomorphology* (Vol. 7) (pp. 212–216). Mountain and Hillslope Geomorphology. <https://doi.org/10.1016/B978-0-12-374739-6.00167-6>
- Currie, A. M., Sands, T. B., & Porter, P. R. (2009). Geotechnical controls on a steep lateral moraine undergoing paraglacial slope adjustment. In J. Knight, & S. Harrison (Eds.), *Periglacial and paraglacial processes and environments. The Geological Society, London, Special Publications* (Vol. 320) (pp. 181–197). <https://doi.org/10.1144/SP320.12>
- Delaloye, R., Lambiel, C., & Gärtner-Roer, I. (2010). Overview of rock glacier kinematics research in the Swiss Alps. *Geographica Helvetica*, 65, 135–145. <https://doi.org/10.5194/gh-65-135-2010>
- Deline, P. (2005). Change in surface debris cover on Mont Blanc massif glaciers after the Little Ice Age termination. *The Holocene*, 15, 302–309. <https://doi.org/10.1191/0959683605hl809rr>
- Dikau, R. (2013). Mass-movement causes: Water. In: Stoffel M, Marston R A. (Dir.). In *Treatise on geomorphology* (Vol. 7) (pp. 207–211). <https://doi.org/10.1016/B978-0-12-374739-6.00166-4>
- Draebing, D., Krautblatter, M., & Dikau, R. (2014). Interaction of thermal and mechanical processes in steep permafrost rock walls: A conceptual approach. *Geomorphology*, 226, 226–235. <https://doi.org/10.1016/j.geomorph.2014.08.009>
- Duvillard, P. A., Ravanel, L., & Deline, P. (2015). Risk assessment of infrastructure destabilisation due to global warming in the high French Alps. *Journal of Alpine Research*, 103. <https://doi.org/10.4000/rga.2896>
- Eggert, D. W., Fitzgibbon, A. W., & Fisher, R. B. (1998). Simultaneous registration of multiple range views for use in reverse engineering of CAD models. *Computer Vision and Image Understanding*, 69, 253–272. <https://doi.org/10.1006/cviu.1998.0667>
- Emmert, A., & Kneisel, C. (2017). Internal structure of two alpine rock glaciers investigated by quasi-3-D electrical resistivity imaging. *The Cryosphere*, 11, 841–855. <https://doi.org/10.5194/tc-11-841-2017>
- Escher, A. (1988). Structure de la nappe du Grand Saint-Bernard entre le val de Bagnes et les Mischabel. National Hydrological and Geological Survey, Bern, Switzerland. Geological Report 7, 26 p.
- Ewertowski, M. W., & Tomczyk, A. M. (2015). Quantification of the ice-cored moraines' short-term dynamics in the high-Arctic glaciers Ebbabreen and Ragnarbrean, Petuniabukta, Svalbard. *Geomorphology*, 234, 211–227. <https://doi.org/10.1016/j.geomorph.2015.01.023>
- Fischer, L., Purves, R. S., Huggel, C., Noetzli, J., & Haeberli, W. (2012). On the influence of topographic, geological and cryospheric factors on rock avalanches and rockfalls in high-mountain areas. *Natural Hazards and Earth System Sciences*, 12, 241–254. <https://doi.org/10.5194/nhess-12-241-2012>

- Geertsema, M., & Chiarle, M. (2013). Mass-movement causes: Glacier thinning. In: Stoffel M, Marston RA. (dir.). In *Treatise on geomorphology* (Vol. 7) (pp. 217–222). Mountain and Hillslope Geomorphology. <https://doi.org/10.1016/B978-0-12-374739-6.00168-8>
- Glaciological reports (1881–2017). The Swiss glaciers. Yearbooks of the Cryospheric Commission of the Swiss Academy of Sciences (SCNAT) published since 1964 by the Laboratory of Hydraulics, Hydrology and Glaciology (VAW) of ETH Zürich, no. 1–136, <http://www.glamos.ch>
- Gorbunov, A. P., & Seversky, E. V. (1999). Solifluction in the mountains of central Asia: distribution, morphology, processes. *Permafrost and Periglacial Processes*, 10, 81–89. [https://doi.org/10.1002/\(SICI\)1099-1530\(199901/03\)10:1<81::AID-PPP307>3.0.CO;2-3](https://doi.org/10.1002/(SICI)1099-1530(199901/03)10:1<81::AID-PPP307>3.0.CO;2-3)
- Gordon, S., Lichti, D. D., Stewart, M. P., & Tsakiri, M. (2000). Metric performance of a high-resolution laser scanner. *Proc. SPIE 4309, Videometrics and Optical Methods for 3D Shape Measurement*, pp. 174–184. DOI: <https://doi.org/10.1117/12.410872>
- Gouffon, Y., & Burri, M. (1997). Les nappes des Pontis, de Siviez-Mischabel et du Mont Fort dans les vallées de Bagnes, d'Entremont et d'Aoste. *Eclogae Geologicae Helvetiae*, 90, 1–177. 0012-9402/97/010029-13
- Gruber, S., & Haeberli, W. (2007). Permafrost in steep bedrock slopes and its temperature-related destabilization following climate change. *Journal of Geophysical Research*, 112, L000547. <https://doi.org/10.1029/2006JF000547>
- Gumus, K., & Erkaya, H. (2011). Analyzing the geometric accuracy of simple shaped reference object models created by terrestrial laser scanners. *International Journal of Physical Sciences*, 6, 6529–6536. <https://doi.org/10.5897/IJPS11.344>
- Haeberli, W. (1992). Construction, environmental problems and natural hazards in periglacial mountain belts. *Permafrost and Periglacial Processes*, 3, 111–124. <https://doi.org/10.1002/ppp.3430030208>
- Haeberli, W., Hallet, B., Arenson, L., Elconin, R., Humlum, O., Kääb, A., ... Vonder Mühl, D. (2006). Permafrost creep and rock glacier dynamics. *Permafrost and Periglacial Processes*, 17, 189–214. <https://doi.org/10.1002/ppp.561>
- Haeberli, W., Noetzli, J., Arenson, L., Delaloye, R., Gärtner-Roer, I., Gruber, S., ... Phillips, M. (2010). Mountain permafrost: Development and challenges of a young research field. *Journal of Glaciology*, 56, 1043–1058. <https://doi.org/10.3189/002214311796406121>
- Haeberli, W., & Vonder Mühl, D. (1996). On the characteristics and possible origins of ice in rock glacier permafrost. *Zeitschrift für Geomorphologie*, 104, 43–57.
- Harris, C., Arenson, L. U., Christiansen, H. H., Etzelmüller, B., Frauenfelder, R., Gruber, S., ... Vonder Mühl, D. (2009). Permafrost and climate in Europe: Geomorphological impacts, hazard assessment and geotechnical response. *Earth-Science Reviews*, 92, 117–171. <https://doi.org/10.1016/j.earscirev.2008.12.002>
- Harrison, S. (2009). Climate sensitivity: implications for the response of geomorphological systems to future climate change. *Geological Society, London, Special Publications*, 320, 257–265. <https://doi.org/10.1144/SP320.16>
- Hauck, C., Vonder Mühl, D., & Maurer, H. R. (2003). Using DC resistivity tomography to detect and characterize mountain permafrost. *Geophysical Prospecting*, 51, 273–284. <https://doi.org/10.1046/j.1365-2478.2003.00375.x>
- Hilbich, C., Marescot, L., Hauck, C., Loke, M. H., & Mäusbacher, R. (2009). Applicability of electrical resistivity tomography monitoring to coarse blocky and ice-rich permafrost landforms. *Permafrost and Periglacial Processes*, 20, 269–284. <https://doi.org/10.1002/ppp.652>
- Hodgetts, D. (2009). LiDAR in the environmental sciences: Geological applications. In G. L. Heritage, & A. R. G. Large (Eds.), *Laser scanning for the environmental sciences* (pp. 165–179). Chichester, UK: Wiley-Blackwell. <https://doi.org/10.1002/9781444311952.ch11>
- Jaboyedoff, M., Oppikofer, T., Abellán, A., Derron, M. H., Loyer, A., Metzger, R., & Pedrazzini, A. (2012). Use of LiDAR in landslide investigations: A review. *Natural Hazards*, 61, 5–28. <https://doi.org/10.1007/s11069-010-9634-2>
- Jäger, D., & Winkler, S. (2012). Paraglacial processes on the glacier foreland of Vernagtferner (Ötztal Alps, Austria). *Zeitschrift für Geomorphologie Supplementary Issue*, 56, 95–113. <https://doi.org/10.1127/0372-8854/2012/S-00099>
- Kääb, A., Reynolds, J. M., & Haeberli, W. (2005). Glacier and permafrost hazards in high mountains. In U. M. Huber, et al. (Eds.), *Global change and mountain regions* (pp. 225–234).
- Kjær, K. H., & Krüger, J. (2001). The final phase of dead-ice moraine development: Processes and sediment architecture, Kötlujökull, Iceland. *Sedimentology*, 48, 935–952. <https://doi.org/10.1046/j.1365-3091.2001.00402.x>
- Kneisel, C. (2003). Permafrost in recently deglaciated glacier forefields—Measurements and observations in the eastern Swiss Alps and northern Sweden. *Z. Geomorph. N. F.*, 47(3), 289–305.
- Knight, J., & Harrison, S. (2012). Evaluating the impacts of global warming on geomorphological systems. *Ambio*, 41, 206–210. <https://doi.org/10.1007/s13280-011-0178-9>
- Kromer, R. A., Abellán, A., Hutchinson, D. J., Lato, M., Edwards, T., & Jaboyedoff, M. (2015). A 4D filtering and calibration technique for small-scale point cloud change detection with a terrestrial laser scanner. *Remote Sensing*, 7, 13029–13052. <https://doi.org/10.3390/rs71013029>
- Kulessa, B. (2007). A critical review of the low-frequency electrical properties of ice sheets and glaciers. *Journal of Environmental and Engineering Geophysics*, 12, 23–36. <https://doi.org/10.2113/JEEG12.1.23>
- Lambiel, C. (2006). Le pergélisol dans les terrains sédimentaires à forte déclivité: distribution, régime thermique et instabilités. PhD Thesis, Université de Lausanne, Lausanne, Switzerland, 260 p. [https://doc.rero.ch/record/6234/files/These\\_LambielC.pdf](https://doc.rero.ch/record/6234/files/These_LambielC.pdf)
- Lambiel, C., & Baron, L. (2008). Two-dimensional geoelectrical monitoring in an alpine frozen moraine. In L. K. Douglas, & K. M. Hinkel (Eds.), *Proceedings of the 9th International Conference on Permafrost* (pp. 161–162). Alaska: Fairbanks. <http://research.iarc.uaf.edu/NICOP/DVD/1st%20to%209th%20Conference%20PDF%20files/09th%20International%20Conference%20on%20Permafrost%20Extended%20Abstracts.pdf>
- Lambiel, C., & Schuetz, P. (2008). Ground characteristics and deformation of a frozen moraine affected by tourist infrastructures (Col des Gentianes, Valais). *Klimaveränderungen auf der Spur. Studien des Europäischen Tourismus Instituts an der Academia Engiadina, Samedan* 5: 110–122. [https://serval.unil.ch/resource/serval:BIB\\_71A3AFFE2F9E.P001/REF](https://serval.unil.ch/resource/serval:BIB_71A3AFFE2F9E.P001/REF)
- Lane, S. N., Chandler, J. H., & Richards, K. S. (1994). Developments in monitoring and modeling small-scale river bed topography. *Earth Surface Processes and Landforms*, 19, 349–368. <https://doi.org/10.1002/esp.3290190406>
- Lane, S. N., Westaway, R. M., & Hicks, D. M. (2003). Estimation of erosion and deposition volumes in a large, gravel-bed, braided river using synoptic remote sensing. *Earth Surface Processes and Landforms*, 28, 249–271. <https://doi.org/10.1002/esp.483>
- Lichti, D. D., Gordon, S. J., & Tipdecho, T. (2005). Error models and propagation in directly georeferenced terrestrial laser scanner network. *Journal of Surveying Engineering*, 131, 135–142.
- Lichti, D. D., & Harvey, B. R. (2002). The effects of reflecting surface material properties on time-of-flight laser scanner measurements. *Symposium on Geospatial Theory, Processing and Application*, Ottawa, pp. 1–9.
- Lichti, D. D., & Licht, M. G. (2006). Experiences with terrestrial laser scanner modelling and accuracy assessment. *International Society for Photogrammetry and Remote Sensing*, 36, 155–160. [http://www.isprs.org/proceedings/XXXVI/part5/paper/LICH\\_614.pdf](http://www.isprs.org/proceedings/XXXVI/part5/paper/LICH_614.pdf)
- Loke, M. H., & Barker, R. D. (1996). Practical technique for 3D resistivity surveys and data inversion. *Geophysical Prospecting*, 44, 499–523. <https://doi.org/10.1111/j.1365-2478.1996.tb00162.x>
- Luethi, R., & Phillips, M. (2016). Challenges and solutions for long-term permafrost borehole temperature monitoring and data interpretation.

- Geographica Helvetica*, 71, 121–131. <https://doi.org/10.5194/gh-71-121-2016>
- Lukas, S. (2011). Ice-cored moraines. In V. P. Singh, P. Singh, & U. K. Haritashya (Eds.), *Encyclopedia of snow, ice and glaciers* (pp. 616–619). Springer, Dordrecht: Encyclopedia of Earth Sciences Series. [https://doi.org/10.1007/978-90-481-2642-2\\_666](https://doi.org/10.1007/978-90-481-2642-2_666)
- Lukas, S., Nicholson, L. I., Ross, F. H., & Humlum, O. (2005). Formation, meltout processes and landscape alteration of high-Arctic ice-cored moraines. Examples from Nordenskiöld Land, Central Spitsbergen. *Polar Geography*, 29, 157–187. <https://doi.org/10.1080/789610198>
- Magnin, F., Krautblatter, M., Deline, P., Ravanel, L., Malet, E., & Bevington, A. (2015). Determination of warm, sensitive permafrost areas in near-vertical rockwalls and evaluation of distributed models by electrical resistivity tomography. *Journal of Geophysical Research*, 120, 745–762. <https://doi.org/10.1002/2014JF003351>
- Matsuoka, N. (2001). Solifluction rates, processes and landforms: A global review. *Earth-Science Reviews*, 55, 107–134. [https://doi.org/10.1016/S0012-8252\(01\)00057-5](https://doi.org/10.1016/S0012-8252(01)00057-5)
- McColl, S. T. (2012). Paraglacial rock-slope stability. *Geomorphology*, 153, 1–16. <https://doi.org/10.1016/j.geomorph.2012.02.015>
- McColl, S. T., & Davies, T. R. H. (2013). Large ice-contact slope movements: Glacial buttressing, deformation and erosion. *Earth Surface Processes and Landforms*, 38, 1102–1115. <https://doi.org/10.1002/esp.3346>
- Milan, D. J., Heritage, G. L., & Hetherington, D. (2007). Application of a 3D laser scanner in the assessment of erosion and deposition volumes and channel change in a proglacial river. *Earth Surface Processes and Landforms*, 32, 1657–1674. <https://doi.org/10.1002/esp.1592>
- Mortara, G., & Chiarle, M. (2005). Instability of recent moraines in the Italian Alps. Effects of natural processes and human intervention having environmental and hazard implications. *Giornale di Geologia Applicata*, 1, 139–146. <https://doi.org/10.1474/GGA.2005-01.0-14.0014>
- Nobes, D. C. (2011). Ground penetrating radar measurements over glaciers. In V. P. Singh, P. Singh, & U. K. Haritashya (Eds.), *Encyclopedia of snow, ice and glaciers* (pp. 490–503). Springer, Dordrecht: Encyclopedia of Earth Sciences Series. [https://doi.org/10.1007/978-90-481-2642-2\\_230](https://doi.org/10.1007/978-90-481-2642-2_230)
- Orlemans, J. (2005). Extracting a climate signal from 169 glacier records. *Science*, 308, 675–677. <https://doi.org/10.1126/science.1107046>
- Oppikofer, T., Jaboyedoff, M., Blikra, L., Derron, M. H., & Metzger, R. (2009). Characterization and monitoring of the Åknes rockslide using terrestrial laser scanning. *Natural Hazards and Earth System Sciences*, 9, 1003–1019. <https://doi.org/10.5194/nhess-9-1003-2009>
- Oppikofer, T., Jaboyedoff, M., & Keusen, H. R. (2008). Collapse at the eastern Eiger flank in the Swiss Alps. *Nature Geoscience*, 1, 531–535. <https://doi.org/10.1038/ngeo258>
- Østrem, G. (1959). Ice melting under a thin layer of moraine and the existence of ice cores in moraine ridges. *Geografiska Annaler*, 41, 228–230.
- PERMOS (2016). In J. Noetzi, R. Luethi, & B. Staub (Eds.), *Permafrost in Switzerland 2010/2011 to 2013/2014. Glaciological Report Permafrost 12–15 of the Cryospheric Commission of the Swiss Academy of Sciences* (p. 85). <http://www.permos.ch/downloads/permos10-14.pdf>
- Phillips, M., Ladner, F., Müller, M., Sambeth, U., Sorg, J., & Teyssiere, P. (2007). Monitoring and reconstruction of a chairlift midway station in creeping permafrost terrain, Grächen, Swiss Alps. *Cold Regions Science and Technology*, 47, 32–42. <https://doi.org/10.1016/j.coldregions.2006.08.014>
- Rabatel, A., Deline, P., Jalliet, S., & Ravanel, L. (2008). Rock falls in high-alpine rock walls quantified by terrestrial LiDAR measurements: A case study in the Mont-Blanc area. *Geophysical Research Letters*, 35, L10502. <https://doi.org/10.1029/2008GL033424>
- Ravanel, L., Allignol, F., Deline, P., Gruber, S., & Ravello, M. (2010). Rockfalls in the Mont Blanc massif in 2007 and 2008. *Landslides*, 7, 493–501. <https://doi.org/10.1007/s10346-010-0206-z>
- Ravanel, L., Bodin, X., & Deline, P. (2014). Using terrestrial laser scanning for the recognition and valorisation of high-alpine geomorphosites. *Geoheritage*, 6, 129–140. <https://doi.org/10.1007/s12371-014-0104-1>
- Ravanel, L., & Deline, P. (2011). Climate influence on rockfalls in high-Alpine steep rockwalls: The north side of the Aiguilles de Chamonix (Mont Blanc massif) since the end of the Little Ice Age. *The Holocene*, 21, 357–365. <https://doi.org/10.1177/0959683610374887>
- Ravanel, L., Deline, P., & Jalliet, S. (2011). Quantification des éboulements/écroulements dans les parois de la haute montagne alpine—Quatre années de laser scanning terrestre dans le massif du Mont-Blanc. *Revue Française de Photogrammétrie et de Télédétection*, 192, 58–65.
- Ravanel, L., Deline, P., Lambiel, C., & Vincent, C. (2012). Instability of a highly vulnerable high alpine rock ridge: The lower Arête des Cosmiques (Mont Blanc massif, France). *Geografiska Annaler A*, 95, 51–66. <https://doi.org/10.1111/geoa.12000>
- Ravanel, L., Magnin, F., & Deline, P. (2017). Impacts of the 2003 and 2015 summer heat waves on permafrost-affected rockwalls in the Mont Blanc massif. *Science of the Total Environment*, 609, 132–143. <https://doi.org/10.1016/j.scitotenv.2017.07.055>
- Reshetnyuk, J. (2006). Investigation and calibration of pulsed time-of-flight terrestrial laser scanners. Licentiate thesis in Geodesy, Royal Institute of Technology (KTH), Department of Transport and Economics, Division of Geodesy, Stockholm, 152 p. <http://citeseerx.ist.psu.edu/viewdoc/download?doi=10.1.1.107.4137&rep=rep1&type=pdf> [http://research.iarc.uaf.edu/NICOP/DVD/ICOP%202003%20Permafrost/Pdf/Chapter\\_166.pdf](http://research.iarc.uaf.edu/NICOP/DVD/ICOP%202003%20Permafrost/Pdf/Chapter_166.pdf)
- Reynard, E., Lambiel, C., Delaloye, R., Devaud, G., Baron, L., Chapellier, D., et al. (2003). Glacier/permafrost relationships in forefields of small glaciers (Swiss Alps). In M. Phillips, S. M. Springman, & L. U. Arenson (Eds.), *Proceedings of the 8th International Conference on Permafrost* (Vol. 1) (pp. 947–952). Zurich.
- Ribolini, A., Guglielmin, M., Fabre, D., Bodin, X., Marchisio, M., Sartini, S., ... Schoeneich, P. (2010). The internal structure of rock glaciers and recently deglaciated slopes as revealed by geoelectrical tomography: Insights on permafrost and recent glacial evolution in the Central and Western Alps (Italy-France). *Quaternary Science Reviews*, 2, 507–521. <https://doi.org/10.1016/j.quascirev.2009.10.008>
- Sailer, R., Bollmann, E., Hoinkes, S., Rieg, L., Sproß, M., & Stötter, J. (2012). Quantification of geomorphodynamics in glaciated and recently deglaciated terrain based on airborne laser scanning data. *Geografiska Annaler A*, 94, 17–32. <https://doi.org/10.1111/j.1468-0459.2012.00456.x>
- Schaer, J. P. (1960). *Géologie de la partie septentrionale de l'éventail de Bagnes*. (p. 148). Switzerland: Thesis, Université de Neuchâtel. <http://doc.rero.ch/record/4448>
- Schomacker, A. (2008). What controls dead-ice melting under different climate conditions? A discussion. *Earth-Science Reviews*, 90, 103–113. <https://doi.org/10.1016/j.earscirev.2008.08.003>
- Schomacker, A., & Kjær, K. H. (2008). Quantification of dead-ice melting in ice-cored moraines at the high-Arctic glacier Holmstrømbreen, Svalbard. *Boreas*, 37, 211–225. <https://doi.org/10.1111/j.1502-3885.2007.00014.x>
- Schulz, T., & Ingensand, H. (2004). Influencing variables, precision and accuracy of terrestrial laser scanners. INGEO 2004 and FIG Regional Central and Eastern European Conference on Engineering Surveying, Bratislava, Slovakia, 8 p. [http://www-group.slac.stanford.edu/met/Align/Laser\\_Scanner/SchulzT\\_TS2\\_Bratislava\\_2004.pdf](http://www-group.slac.stanford.edu/met/Align/Laser_Scanner/SchulzT_TS2_Bratislava_2004.pdf)
- Shumskii, P. A. (1964). *Principles of structural glaciology*. New York: Dover Publications Inc. 497 p
- Springman, S. M., Arenson, L. U. (2008). Recent advances in permafrost geotechnics. Proceedings of the 9<sup>th</sup> International Conference on Permafrost, Fairbanks, Alaska 2: 1685–1694. <http://research.iarc.uaf.edu/NICOP/DVD/1st%20to%209th%20Conference%20PDF%20files/09th%20International%20Conference%20on%20Permafrost%20Vol%202.pdf>

- Thompson, S., Kulessa, B., & Luckmann, A. (2012). Integrated electrical resistivity tomography (ERT) and self-potential (SP) techniques for assessing hydrological processes within glacial lake moraine dams. *Journal of Glaciology*, 58, 849–858. <https://doi.org/10.3189/2012JoG11J235>
- Tonkin, T. N., Midgley, N. G., Cook, S. J., & Graham, D. J. (2016). Ice-cored moraine degradation mapped and quantified using an unmanned aerial vehicle: A case study from a polythermal glacier in Svalbard. *Geomorphology*, 258, 1–10. <https://doi.org/10.1016/j.geomorph.2015.12.019>
- Van Den Eeckhaut, M., Poesen, J., & Hervás, J. (2013). Mass-movement causes: Overloading. In: Stoffel M, Marston RA. (dir.). In *Treatise on geomorphology* (Vol. 7) (pp. 200–206). Mountain and Hillslope Geomorphology. <https://doi.org/10.1016/B978-0-12-374739-6.00165-2>
- Wheaton, J. M., Brasington, J., Darby, S. E., & Sear, D. A. (2010). Accounting for uncertainty in DEMs from repeat topographic surveys: Improved sediment budgets. *Earth Surface Processes and Landforms*, 35, 136–156. <https://doi.org/10.1002/esp.1886>
- Young, A. P., & Ashford, S. A. (2006). Application of airborne LiDAR for seaciff volumetric change and beach-sediment budget contribution. *Journal of Coastal Research*, 22, 307–318. [https://www.cdip.ucsd.edu/themes/media/docs/publications/journal\\_articles/Young\\_and\\_Ashford\\_JCR\\_2006.pdf](https://www.cdip.ucsd.edu/themes/media/docs/publications/journal_articles/Young_and_Ashford_JCR_2006.pdf)
- Zemp, M., Frey, H., Gärtner-Roer, I., Nussbaumer, S. U., Hoelzle, M., Paul, F., ... Vincent, C. (2015). Historically unprecedented global glacier decline in the early 21<sup>st</sup> century. *Journal of Glaciology*, 61, 745–762. <https://doi.org/10.3189/2015JoG15J017>
- Zhao, N. Z., Yan, L., Zhao, Y. S., Lv, Y. F., & Wu, T. X. (2007). Multi-factor analysis of reflection from granite surfaces. *Journal of China University of Mining and Technology*, 17, 255–257. [https://doi.org/10.1016/S1006-1266\(07\)60083-2](https://doi.org/10.1016/S1006-1266(07)60083-2)

**How to cite this article:** Ravanel L, Duvillard P-A, Jaboyedoff M, Lambiel C. Recent evolution of an ice-cored moraine at the Gentianes Pass, Valais Alps, Switzerland. *Land Degrad Dev*. 2018;29:3693–3708. <https://doi.org/10.1002/lrd.3088>